Project no. 248992

Project acronym: NEUNEU

Project title: Artificial Wet Neuronal Networks from Compartmentalised Excitable Chemical Media

Small or medium-scale focused research project (STREP)

Deliverable 4.1 - Software model of synaptic connection between two BZ-droplets

Period covered: from 1.2.2010 to 29.2.2012 Date of preparation: 18.9.2009

Start date of project: 1.2.2010 Duration: 36 months

Project coordinator name: Dr. Peter Dittrich
Project coordinator organisation name: Friedrich Schiller University Jena

Logical and arithmetic circuits in Belousov-Zhabotinsky encapsulated disks

Julian Holley,[1,*] Ishrat Jahan,[2] Ben De Lacy Costello,[2] Larry Bull,[1] and Andrew Adamatzky[1]
[1]*Faculty of Environment and Technology, University of the West of England, Bristol, England*
[2]*School of Life Sciences, University of the West of England, Bristol, England*
(Received 3 June 2011; revised manuscript received 26 September 2011; published 23 November 2011)

Excitation waves on a subexcitable Belousov-Zhabotinsky (BZ) substrate can be manipulated by chemical variations in the substrate and by interactions with other waves. Symbolic assignment and interpretation of wave dynamics can be used to perform logical and arithmetic computations. We present chemical analogs of elementary logic and arithmetic circuits created entirely from interconnected arrangements of individual BZ encapsulated cell-like disk. Interdisk wave migration is confined in carefully positioned connecting pores. This connection limits wave expansion and unifies the input-output characteristic of the disks. Circuit designs derived from numeric simulations are optically encoded onto a homogeneous photosensitive BZ substrate.

DOI: 10.1103/PhysRevE.84.056110 PACS number(s): 82.40.Ck, 89.20.Ff, 89.75.Fb, 89.75.Kd

I. INTRODUCTION

Unconventional computing [1] is a field of study dedicated to exploring alternate computational strategies, structures, and media, in contrast to contemporary digital von Neumann architecture machines [2]. Innate serial execution and storage processing of these machines present profound throughput and energy restrictions, limiting practical application of some classes of algorithms [3]. Conversely, computation-capable organic adaptive systems are innately parallel and distributed. Highly parallel and distributed computation can be supported in chemical reaction-diffusion (RD) systems [4] such as the Belousov-Zhabotinsky (BZ) reaction [5]. One benchmark of these systems is the ability to replicate components used in conventional computation, such as logic and arithmetic circuits. Logic gates are the physical embodiment of Boolean logic operations that form the foundation for digital computation. Circuits of logic gates can be connected to create machines capable of performing *universal computation* [6].

The chemical implementation of logic gates was first described by Rossler, who sustained gates in a bistable chemical medium [7]. Logic gates have also been demonstrated using chemical kinetics [8–11]. The binary value assignment to the presence or absence of individual RD waves modulated by the substrate geometry and other waves presents an alternative approach. Toth first described logic gates with BZ waves along these lines [12,13]. In that system RD waves traveled along thin capillary tubes. These basic principles have since led to numerous adaptations; for example, Steinbock implemented logic gates by "printing" a catalyst of the BZ reaction onto a facilitating medium [14]. In a simulated study Motoike presented (among other designs) logic gates reliant upon geometric patterns of passive diffusion boundaries embedded on an excitable field [15]. Sielewiesiuk also created logical functions by using passive diffusion lines where function arose at the intersection of perpendicular wave channels [16]. Adamatzky presented alternative logic gate designs by combining the principles of collision-based computing on an precipitating chemical substrate [17,18] and *in vitro* [19]. Similar or derived studies—such as the FitzHugh-Nagumo model [20–22] reaction, a coevolutionary system [23], a cardiac cell model on a Graphics Processing Unit (GPU) [24], and others [25]—have all implemented logic functions or gates either in simulation, *in vitro*, or both.

Current experiments with lipid-coated vesicles of excitable media at our (and our partners [26]) laboratories have led to a geometric BZ-mediated approach to creating logic and arithmetic functions. By representating of a two-dimensional approximation of BZ vesicles, networks of interconnected disks containing a subexcitable BZ formulation can be arranged to create various circuits. Logic and arithmetic circuits and polymorphic gates have been simulated in homogeneous hexagonal and orthogonal networks [27–29] and in nonhomogeneous arrangements [30].

In these simulations, geometric arrangements of disks are joined together by small connecting pores. The resulting pattern modulates a homogeneous BZ Oregonator simulation grid that has been adapted for monochromatic photosensitivity [31]. The disk boundaries are created from rings of high-intensity light to emulate an impenetrable exterior membrane. Lower-intensity light forms the interior disk area, and connecting pores are adjusted to support traveling waves.

Logically symbolic waves are able to traverse the network modulated by interaction with pathways and other waves. The disk interior can be exploited for free-space collision-style reactions [17], whereas the pore loci and efficiency can compartmentalize the resulting reaction [27]. Circuits have been created from logical subassembles in orthogonal and hexagonal networks [27,30]. Function density can be increased by circuits that include variations in relative disk size, pore efficiency, and connection angles [30]. Using this latter technique we have assembled a compact elementary arithmetic circuit.

Conceivably other cell geometries (such a grids of square units) could compartmentalize cell function similar to disks. Nevertheless, the curvature of the wave front in combination with the disk geometry provides a natural and convenient unit and network structure. In comparison to our previous free-space [32] or channeled-logic optically projected circuits [33], the combination of the natural positively expanding wave curvature and the disk geometry promotes functional interdisk stability and connectivity.

*julian2.holley@uwe.ac.uk; http://uncomp.uwe.ac.uk/holley

Use of a photosensitive-adapted version of the Oregonator model permits a simple migration from simulation to experiment. Circuit designs from the simulation can be projected directly onto an actual photosensitive BZ medium. Furthermore, the same substrate is capable of supporting different successive circuits. Detected activity in assigned output disks can trigger the projection of alternate circuits onto the same substrate area. Those triggering waves can be *captured* into the circuit, effectively becoming inputs into the new circuit. Migration of our stabilizing disk-centric circuit simulations onto a reusable chemical substrate is the primary subject of this paper.

II. METHODS

Designs are initially created in simulation and then the resulting geometry is projected onto the BZ substrate. This substrate is a photosensitive BZ system [34] with a $Ru(bpy)_3^{3+}$ catalyst immobilized on silica gel [35]. The medium is oscillatory in the dark with composition as described in Ref. [36]. Global illumination levels are manually adjusted to promote marginal excitation waves. Simultaneous multiple wave initiations are optically instigated. Removing all inhibiting light promotes mass wave excitation across the BZ substrate. Normal light levels and the experimental pattern are then restored, with the exception of small circular zones at desired initiation points. Wave fragments continue to emerge from these dark zones out into the marginal zone of the disk body.

A. Numerical simulation

Numerical simulations are based on a two-variable version of the Oregonator model [37] as a model of the BZ reaction [5, 38] adapted for photosensitive modulation of the Ru-catalyzed reaction [31]:

$$\frac{\partial u}{\partial t} = \frac{1}{\epsilon}\left[u - u^2 - (fv + \phi)\frac{u - q}{u + q}\right] + D_u \nabla^2 u, \qquad \frac{\partial v}{\partial t} = u - v. \tag{1}$$

Variables u and v are the local instantaneous dimensionless concentrations of the bromous acid autocatalyst activator $HBrO_2$ and the oxidized form of the catalyst inhibitor $Ru(bpy)_3^{3+}$. ϕ symbolizes the rate of bromide production proportional to applied light intensity. Bromide Br^- is an inhibitor of the Ru-catalyzed reaction, therefore excitation can be modulated by light intensity; high-intensity light inhibits the reaction. Dependent on the rate constant and reagent concentration, ϵ represents the ratio of the time scales of the two variables u and v. q is a scaling factor dependent on the reaction rates alone. The diffusion coefficients D_u and D_v of u and v were set to unity and zero respectively. The coefficient D_v is set to zero because it is assumed that the diffusion of the catalyst is limited. Inputs where instigated by perturbing the activator $u = 1.0$ centrally in small circular disk areas, with a radius of 2 simulation points (SPs).

Numerical simulations were achieved by integrating the equations using the Euler alternating-direction implicit (ADI) method [39] with a time step $\delta t = 0.001$ and a spatial step $\delta = 0.25$. Experimental parameters are given in Table I.

TABLE I. Kinetic and numerical values used in numerical simulations of Eq. (1).

Parameter	Value	Description
ϵ	0.022	Ratio of time scale for variables u and v
q	0.0002	Propagation scaling factor
f	1.4	Stoichiometric coefficient
ϕ	[a]	Excitability level (proportional to light level)
u	–	Activator $HBrO_2$
v	–	Inhibitor $Ru(bpy)_3^{3+}$
D_u	1.0	Activator diffusion coefficient
D_v	0	Inhibitor diffusion coefficient
Δx	0.25	Spatial step
Δt	0.001	Time step

[a] ϕ varies between two levels, subexcited ($L1$) and inhibited ($L2$): $\phi_{L1} = 0.076$, $\phi_{L2} = 0.209$.

Networks of disks where created by mapping two different ϕ values (proportional to light intensity) onto a rectangle of homogeneous simulation substrate. To improve simulation performance the rectangle size was automatically adapted depending on the size of the network, but the simulation-point (SP) density remained constant throughout. The excitation levels $L1$ and $L2$ relate to the partially active disk interiors and nonactive substrate.

Disks are always separated by a single simulation-point (1 SP) wide boundary layer. Connection pores between disks are created by superimposing another small *link* disk at the point of connection (typically a radius of 2–6 SP); simulation points have a 1:1 mapping with on-screen pixels. The reagent concentrations are represented by a red and blue color mapping; the activator u is proportional to the red level, and the inhibitor v is proportional to the blue level. The color graduation is automatically calibrated to minimum and maximum levels of concentration over the simulation matrix. The background illumination is monochromatically calibrated in the same fashion proportional to ϕ: white areas are inhibitory, and dark areas excited [for monochromatic reproductions, blue (v) has been suppressed and red (u) appears as light gray; color versions are online].

Wave fragment flow is represented by a series of superimposed time lapse images. Unless stated otherwise, the time lapse is 50 simulation steps. To improve clarity, only the activator (u) wave-front progression is recorded. Figure 1

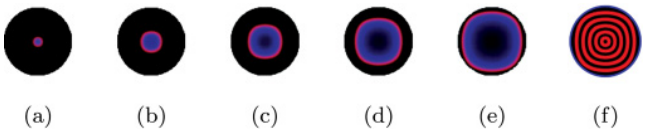

FIG. 1. (Color online) Example of time-lapse image creation. The image shown in (f) is the accumulation of successive images shown from central wave initiation in (a) to extinction in (e). Time lapses periods are 50 time steps and the refractory tail of the inhibitor (u) shown in blue [gray inner shadow of propagating ring in (a)–(e)] is not shown in the time-lapse image (f) to improve clarity.

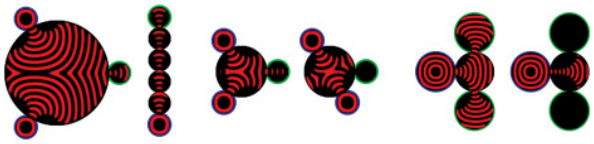

(a)Relative disc sizes (b)Connection angle (c)Connection efficiency

FIG. 2. (Color online) (a) Disks as reaction vesicles in the left-hand-side network or communication channels in the right-hand-side network. (b) The effect of connection angle; the two input signals combine in the left network to produce an output. Adjusting the angle of the lower input in the right network alters the result of the collision and no output is produced. (c) The effect of connection efficiency. The large-aperture (6 SP) connection in the left network results in a broadly spreading beam. Conversely, a smaller (4 SP) aperture connection in the right network creates a narrow beam wave.

illustrates the same wave fragment in both color map (u and v) and final composite time-lapse version (u).

Inputs are created by perturbing a small circular area of the activator (u) set to a value of 1.0 with a radius of 2 SP in the center of the disk. In addition to explicit labeling, all disks representing inputs and outputs are also highlighted with a blue and green border, respectively.

In a previous study we have shown that logic circuits can be created with uniform disks arranged in hexagonal networks [29], hexagonal packing being the most efficient method of sphere (disk) packing. Further opportunities to modulate wave fragment behavior are presented when disk size, connection angle, and connection efficiency are combined in nonhomogeneous networks. Disk size can be adjusted to permit or restrict internal wave interactions, producing either larger reaction-vessel disks or smaller communications disks [Fig. 2(a)]. The connection angle between disks can be used to direct wave collisions [Fig. 2(b)], and connection efficiency can affect the wave focus [Fig. 2(c)].

B. Experiment

A Sanyo Pro Xtrax Multiverse projector was used to project the design outline of several simulated circuit designs from Ref. [30]. Wave activity was captured using a Lumenera Infinity 2 USB 2.0 scientific digital camera. The open reactor was surrounded by a water jacket regulated at 20 °C. Peristaltic pumps were used to pump the reaction solution into the reactor and remove the effluent (Fig. 3).

Sodium bromate, sodium bromide, malonic acid, sulfuric acid, tris(bipyridyl) ruthenium(II) chloride, and 27% sodium silicate solution stabilized in 4.9M sodium hydroxide [40] were used as received unless stated otherwise. $Ru(bpy)_3^{3+}$ was recrystallized from the choloride salt with sulfuric acid. To create the catalyst-loaded gels, thin-layer-chromatography precoated plates of silica gel with a 254-nm fluorescent indicator on glass were cut into 5×5 cm pieces and placed in 0.9 ml of 0.025M $Ru(bpy)_3^{3+}$ solution and 12 ml of de-ionized water in a Petri dish for 12 h. Gels were washed in de-ionized water to remove by-products before use.

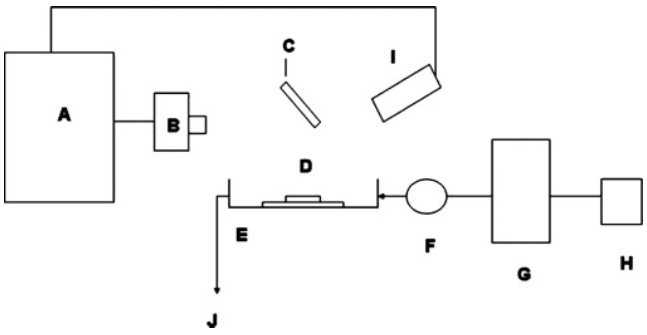

FIG. 3. Experimental setup: A light sensitive catalyst, $Ru(bpy)_3^{3+}$-loaded silica gel, is immersed in catalyst-free BZ reaction solution in a thermostat-controlled (G) Petri dish (E). (F) is a peristaltic pump. A reactor provides thermostat-controlled reaction solution and removes effluent (J). The reaction solution reservoir (H) is kept in an ice bath. The heterogeneous network on the surface of the gel (D) is constructed by the projection (B) of a disk pattern generated by a computer (A) via a mirror assembly (C). Images were captured with a digital camera fitted with a 455-nm narrow-bandpass interference filter (I).

The catalyst-free reaction mixture was freshly prepared in a 30-ml continuously fed stirred-tank reactor (CSTR), which involved the *in situ* synthesis of stoichiometric bromomalonic acid from malonic acid and bromine generated from the partial reduction of sodium bromate. This CSTR in turn continuously fed a thermostat-controlled open reactor with fresh catalyst-free BZ solution in order to maintain a nonequilibrium state. The final composition of the catalyst-free reaction solution in the reactor was 0.42M sodium bromate, 0.19M malonic acid, 0.64M sulfuric acid, and 0.11M bromide. The residence time was 30 min.

The spatially distributed excitable field on the surface of the gel was achieved by the projection of the disk pattern from the simulations. The light intensity of the disks was controlled by computer. The pattern was projected onto the catalyst-loaded gel via a data projector. Every 10 s, a light level of 5.7 mW/cm^2 was applied for 10 ms, during which time an image of the BZ fragments on the gel was captured. The purpose of this was to allow activity on the gel to be more visible to the camera. Captured images were processed to identify chemical activity. This was done by differencing successive images to create a black-and-white image. The images were cropped and layered to show progression of a single image, and finally the disk boundary was superimposed on the images to aid analysis of the results.

III. RESULTS

We report on a selection of experiments that successfully migrated from simulation: a diode, a NAND gate, an XOR gate, and a simple arithmetic adder circuit [30]. In the following images the inverse monochromatic wave progression (left column) is illustrated adjacent to the respective color simulation analog (right column). Although the parametrization of the simulation creates different wave dynamics, the projected geometry in each case is proportionally identical, resulting in the same functionality.

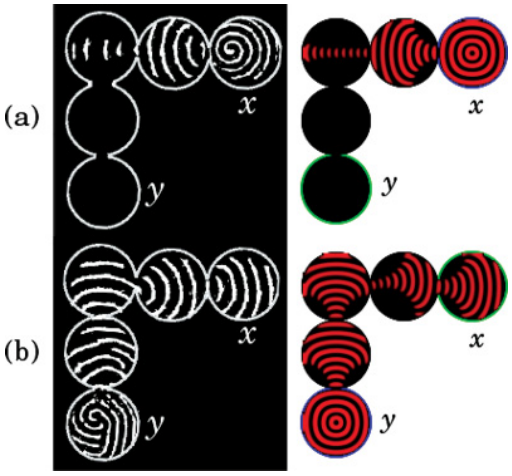

FIG. 4. (Color online) Diode junction ($x \rightarrow y = 0$, $y \rightarrow x = 1$). Left column sequences show wave (signal) development compared alongside analogous numerical simulations on the right. (a) The signal propagates horizontally ($x \rightarrow y$). A narrow-band pore (4 SP) at the second (right-angle) junction prohibits propagation downward to y. (b) The signal propagates vertically ($y \rightarrow x$). A broad-band pore (6 SP) at the second (right-angle) junction connection permits the signal to expand horizontally toward x. The simulation-to-gel projection ratio is 56 SP to 10 mm diameter [42].

A. Diode

The diode junction constructed with BZ disks operates by simultaneously exploiting a right-angle junction and asymmetric pore size (Fig. 4). A wave fragment (y) travels horizontally from right to left [Fig. 4(a)]. Wave fragments cannot survive when the fragment size drops below some critical level [41]. A constricted pore of 4 SP at the perpendicular junction reduces the wave size close to termination in the proceeding disk. Wave development is momentarily marginal before slowly recovering. Delay in wave development prohibits the fragment from entering the vertical connection [42]. Conversely the opposing vertical fragment (y) enters the junction through a broad pore (6 SP). The resultant increased junction wave seed permits the fragment to develop more rapidly and dissipate into the horizontal disks line [Fig. 4(b)]. Therefore signal propagation only progresses from vertical to horizontal ($x \rightarrow y$). Disks in the simulation have a diameter of 56 SP, which results in a projected gel disk of 10 mm diameter. This diode junction has been used to inject unidirectional wave fragments into a type of simulated 1-bit memory where unidirectional waves indefinitely circulate around a loop of disks until reagent exhaustion or collision with an opposing wave [30].

B. NAND logic gate

A NAND gate design is shown in Fig. 5 and animated in the Supplemental Material [42]. The gate is a conjunction of an AND gate and an *inverter* or NOT gate. The NOT gates operates horizontally in the bottom four disks. A logical TRUTH or "1" (supply wave) is always presented simultaneously with the inputs x and y. In the case of $(x,y) = (0,0)$ a wave propagates horizontally unimpeded, terminating in the output disk z ($z = 1$) [Fig. 5(a)]. Input cases $(x,y) = (1,0)$ and $(0,1)$ also have no effect on the progression of the

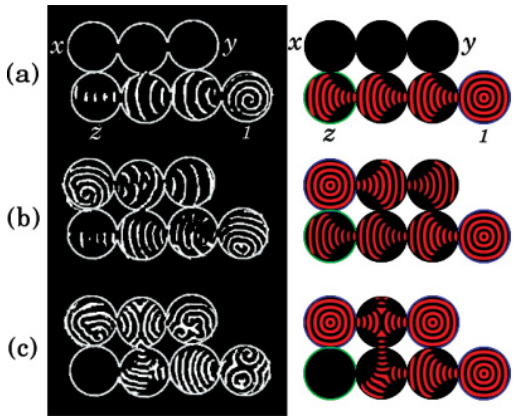

FIG. 5. (Color online) Two input NAND gate ($z = \overline{x \bullet y}$). Left column sequences show wave (signal) development compared alongside numerical simulations on the right. (a) $z = 1$, $(x,y) = [0,0]$. (b) $z = 0$, $(x,y) = [0,1]||[1,0]$. (c) $z = 0$, $(x,y) = [1,1]$. Pores of 6 SP interconnect 56 SP diameter disks with simulation-to-gel projection ratio of 56 SP to 10 mm diameter [42].

supply wave, and in both cases $z = 1$ [Fig. 5(b)]. In the final instance $(x,y) = (1,1)$ the inputs collide in the central disk, resulting in a perpendicular ejection wave. The downward ejection wave fragment propagates into the horizontal NOT line below, deflects, and causes the extinction of the supply wave, leading to a negated output ($z = 0$) [Fig. 5(c)]. The NAND gate is significant because of its universal applicability in the construction of all other logic gates. This design is illustrative of the modular facilitation of BZ disk networks creating a NAND gate from the conjunction of an AND and a NOT gate.

C. XOR logic gate

Figure 6 demonstrates the XOR function. As with the proceeding NAND gate, a logical TRUTH ("1") is supplied in two disks (center top and bottom right) in synchronization with the two inputs (x and y). Input $(x,y) = (0,0)$ allows the vertical supply wave to deflect the horizontal supply wave, resulting in logical false output $z = 0$ [Fig. 6(a)]. Complementary inputs $(x,y) = (0,1)$ and $(1,0)$ deflect the vertically traveling supply wave, allowing the horizontal supply wave to reach the output disk ($z = 1$) [Fig. 6(b)]. Finally, input of $(x,y) = (1,1)$ cancels the effect of the asymmetric collision of the vertical supply wave again deflecting the horizontal wave path ($z = 0$) [Fig. 6(c)] [42].

Using this design strategy we have constructed other simulated gates (NOT, AND, OR, NXOR) and with combinations the we have also simulated simple memory and arithmetic circuits [30].

D. Composite 1-bit half-adder circuit

One of the building blocks of electronic digital arithmetic circuits is the 1-bit half adder (HA). Two HA circuits can be connected to make a full 1-bit adder. One-bit adders can then be repeatedly connected to make an n-bit adder. A successful construction of a HA is therefore demonstrative of the arithmetic capabilities of this scheme. The HA circuit takes two inputs, the n bit (x) in conjunction with a carry (y), and

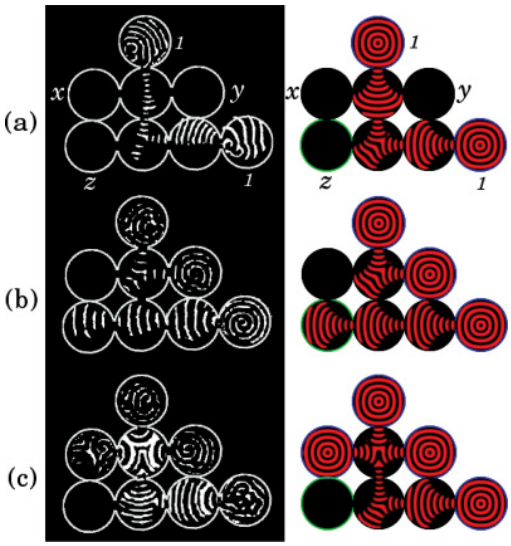

FIG. 6. (Color online) Two input XOR gate ($z = x \oplus y$). Left-column sequences show wave (signal) development compared alongside numerical simulations on the right for the input sets (a) $z = 0$, $(x,y) = [0,0]$, (b) $z = 1$, $(x,y) = [0,1]|[1,0]$, and (c) $z = 0$, $(x,y) = [1,1]$. Pores of 6 SP interconnect 56 SP diameter disks with simulation-to-gel projection ratio of 56 SP to 10 mm diameter [42].

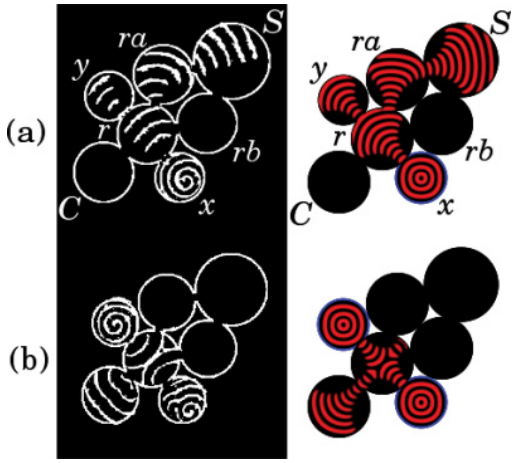

FIG. 7. (Color online) One-bit half-adder circuit ($S = x \oplus y$, $C = x \bullet y$). The central reactor disk performs both XOR and AND logic functions to create the desired logic. (a) XOR component, $S = 1$, $C = 0$, $(x,y) = [0,1]|[1,0]$. (b) AND component, $S = 0$, $C = 1$, $(x,y) = [1,1]$. Pores of 4 SP interconnect disks of 56 SP diameter scaled by 1.2 for S and 0.8 for x and y, with simulation-to-gel projection ratio of 56 SP to 10 mm diameter. The circuit exploits three types of wave modulation: connection angle, disk size, and pore efficiency [42].

produces two outputs, the sum (S) and carry (C). A HA can be constructed from a combination of two logic gates: the XOR and AND gates. There are two inputs (x and y) and two outputs (S and C). The binary sum (S) of x and y is achieved by the XOR gate ($S = x \oplus y$), and inability of the configuration (overflow) to present the $1 + 1$ input is achieved with a carry (C) output ($C = x \bullet y$).

We have simulated several half-adder and full-adder circuits arranged in orthogonal [30] and hexagonal [27] networks where AND and XOR gates form building blocks in a larger circuit. It is possible to increase functional density by adding flexibility. With the exception of the previous diode, the above logic gates are constructed with disks connected with a uniform orthogonal network and connection pores. More efficient designs are possible by permitting flexibility in terms of disk size, connection pore (see diodes) and interdisk connection angle.

Figure 7 illustrates a compact HA circuit design where the XOR and AND gate are combined in a central single *reactor* disk (R). Interconnecting disks ($r1$,$r2$) between the central reactor disk guide wave fragments to the S output to create the XOR feature [$xy(1,0)$ and $xy(0,1) \rightarrow S = 1, C = 0$]. The AND feature is created by the perpendicular wave ejecting fragments directly into C [$xy(1,1) \rightarrow S = 0, C = 1$] [42].

IV. DISCUSSION

In much the same way that electronic circuits are designed and constructed we have created an alternative HA circuit as presented above. In electronics the HA circuit is formed from the conjunction of an AND gate unit and a XOR gate unit. Recursive connections lead to the creation of memory and sequential circuits that can be combined with diodes and logic gates to create other circuits. Beyond the limitations of our own laboratory resources we foresee no barriers to successful migration of these additional circuits.

Although these circuits share some similarities with their electronic counterparts, there are differences. Reagents, the chemical analog of the *power supply*, are embedded and distributed throughout the circuit substrate and not supplied from one source. A circuit can thus activate for short periods in the absence of any reagent refreshment. The vector component of the reaction wave presents another interesting contrast. Temporally separated waves can share a common channel without interference. It is therefore possible to create a "crossroads" junction where wave signals traveling in different directions can share the same substrate without interference [30]. Furthermore, the optical-circuit projection onto a homogeneous substrate permits substrate reuse with preservation of current signals. One operating circuit projection can be instantaneously replaced with another circuit. Waves in target locations could trigger circuit changes and conceivably also incorporate other existing wave signals into the *unique* circuit.

At a scale where excitation waves are visible to the human eye, this BZ reaction diffusion process is relatively slow. In these experiments disks are ~10 mm in diameter and waves propagate at ~0.5 mm/s, resulting in a 20-s propagation delay per disk. Wave-front geometry is an emergent property of the chemical composition and substrate that develops independently of the initiation geometry. Reducing the disk physical dimensions therefore requires an proportionate increase in chemical kinetics to maintain functional equilibrium. For example, if the chemical kinetics could be adapted to reduce the wave-front size, then a reduction in diameter to that of a typical neuron, from 10 to 0.004 mm, could produce at least a linear adjustment in disk propagation delay of

(20 s)/2500 = 8 ms. In comparison the refractory phase of a typical neuron is ∼1 ms.

This research is an exploratory component within a wider collaborative project that aims to create functional networks of lipid encapsulated BZ vesicles [26]. The lipid membrane and the nonlinear oscillatory nature of the BZ medium encodes some of the features apparent in biological information processing; there are systematic analogies between electrobiochemical neurons and BZ disks, such as pores versus synapses and chemical versus electrical excitation and refraction.

V. FUTURE WORK

To demonstrate the computational abilities of BZ encapsulated disks we have combined Boolean information representation and geometric collision style manipulation. The essential components required for a universal computer could be created with this combination. Other modes of information representation and manipulation are possible in these networks. In an oscillatory mode, information could be coded in pulse phase relationships and manipulated by interconnected temporal associations, reminiscent of natural neural information processing. Information is processed probabilistically along the edge of the BZ instability threshold through interconnected membrane pores. Larger reactor chambers could possibly be connected by strings of smaller disks or vesicles.

Our explorations have so far been restricted to two dimensions. Disks have been substituted for cross sections of interconnected vesicles. In future studies we plan to extend our simulations into the third dimension. We speculate that similar modulation of wave *cones* could also be possible leading to three-dimensional vesicle computational or adaptive circuits.

Designing anything beyond the simplest devices in such schemes, as is the case with neural networks, can be uncertain and complex. We intend to create disks capable of adaptation in order to learn solutions, and to employ evolutionary strategies to search for static structural solutions. Currently we are exploring an evolutionary strategy to replicate the functionality of our manual designs of logic gates and arithmetic circuits. Success there opens the possibility of solving computational tasks for which solutions are currently protracted in conventional systems.

VI. CONCLUSION

Concomitant within our long-term project aims, we have developed a prototype information processing system from interconnected arrangements of BZ encapsulated disks as analogs of BZ vesicles. Expanding excitation waves sustained in a subexcitable BZ substrate represent discrete quanta of information. The interconnecting disk pores have a stabilizing effect on the waves as they propagate from one disk to another. Connections, pore efficiency, connection angle, and relative disk size are used to manipulate waves to create explicit chemical information processing devices.

Networks of these units share some features apparent in biological information processing. While interneuron communication is predominately electrical, modulation of that activity is chemical. In the case of individual neurons, modulation dominates at the synaptic junction. The membrane pore between two vesicles can be considered a simple analog of the synapse: a small contact area that can modulate signals in between vesicles. Similarly the electric upstate firing and downstate quiescence of neural signaling is an analog of chemical excitation and refraction.

ACKNOWLEDGMENTS

This work is funded under 7th FWP FET European Project No. 248992. We thank Peter Dittrich, Jerzy Gorecki, and Klaus-Peter Zauner for their inspiration and useful discussions [26]. The authors also acknowledge EPSRC Grant No. EP/E016839/1 in support of Ishrat Jahan.

[1] *Unconventional Computing 2007*, edited by A. Adamatzky, B. De Lacy Costello, L. Bull, S. Stepney, and C. Teuscher (Luniver, Bristol, England, 2006).
[2] *John von Neumann: Selected Letters*, edited by M. Rédei (American Mathematical Society, Providence, 2005).
[3] D. Harel, *Computers Ltd: What They Really Can't Do* (Oxford University Press, London, 2003).
[4] A. Adamatzky, B. De Lacy Costello, and T. Asai, *Reaction-Diffusion Computers* (Elsevier, New York, 2005).
[5] A. M. Zhabotinsky and A. N. Zaikin, J. Theor. Biol. **40**, 45 (1973).
[6] A. Turing, Proc. London Math. Soc. **42**, 230 (1936).
[7] O. E. Rossler, in *Physics and Mathematics of the Nervous System*, edited by M. Conrad, W. Guttinger, and M. Dal (Springer, Berlin, 1974), pp. 399–418.
[8] A. Hjelmfelt, E. D. Weinberger, and J. Ross, Proc. Natl. Acad. Sci. USA **88**, 10983 (1991).
[9] A. Hjelmfelt, E. D. Weinberger, and J. Ross, Proc. Natl. Acad. Sci. USA **89**, 383 (1992).
[10] A. Hjelmfelt, E. D. Weinberger, and J. Ross, Science **260**, 335 (1993).
[11] M. O. Magnasco, Phys. Rev. Lett. **78**, 1190 (1997).
[12] A. Tóth, V. Gaspar, and K. Showalter, J. Phys. Chem. **98**, 522 (1994).
[13] A. Tóth and K. Showalter, J. Chem. Phys. **103**, 2058 (1995).
[14] O. Steinbock, A. Toth, and K. Showalter, Science **267**, 868 (1995).
[15] I. Motoike and K. Yoshikawa, Phys. Rev. E **59**, 5354 (1999).
[16] J. Sielewiesiuk and J. Górecki, J. Phys. Chem. A **105**, 8189 (2001).
[17] A. Adamatzky and B. De Lacy Costello, Phys. Rev. E **66**, 046112 (2002).
[18] A. Adamatzky, Chaos Solitons Fractals **21**, 1259 (2004).
[19] B. De Lacy Costello and A. Adamatzky, Chaos Solitons Fractals **25**, 535 (2005).
[20] I. N. Motoike and A. Adamatzky, Chaos Solitons Fractals **24**, 107 (2005).

[21] R. FitzHugh, Biophys. J. **1**, 445 (1961).
[22] J. Nagumo, S. Arimoto, and S. Yoshizawa, Proc. IRE **50**, 2061 (1962).
[23] C. Stone, R. Toth, B. De Lacy Costello, L. Bull, and A. Adamatzky, in *Parallel Problem Solving from Nature – PPSN X*, edited by G. Rudolph, T. Jansen, S. Lucas, C. Poloni, and N. Beume, Lecture Notes in Computer Science Vol. 5199 (Springer, Berlin, 2008), pp. 579–588.
[24] S. Scarle, Comput. Biol. Chem. **33**, 253 (2009).
[25] J. Górecki and J. N. Górecka, in *Encyclopedia of Complexity and Systems Science*, edited by R. A. Meyers (Springer, Berlin, 2009).
[26] NeuNeu Project, "Artificial Wet Neuronal Networks from Compartmentalised Excitable Chemical Media," [http://neu-n.eu.]
[27] A. Adamatzky, B. De Lacy Costello, L. Bull, and J. Holley, Isr. J. Chem. **51**, 1 (2011).
[28] A. Adamatzky, B. De Lacy Costello, and L. Bull, Int. J. Bifurcation Chaos **21**, 1977 (2011).
[29] A. Adamatzky, J. Holley, L. Bull, and B. De Lacy Costello, Chaos Solitons Fractals **44**, 779 (2011).
[30] J. Holley, A. Adamatzky, L. Bull, B. De Lacy Costello, and I. Jahan, Nano Commun. Networks **2**, 50 (2011).
[31] L. Kuhnert, Nature (London) **319**, 393 (1986).
[32] B. De Lacy Costello and A. Adamatzky, Chaos Solitons Fractals **25**, 535 (2005).
[33] B. De Lacy Costello, A. Adamatzky, I. Jahan, and L. Zhang, Chem. Phys. **381**, 88 (2011).
[34] V. Gáspár, G. Bazsa, and M. T. Beck, Z. Phys. Chem. (Leipzig) **264**, 43 (1983).
[35] J. Wang, S. Kádár, P. Jung, and K. Showalter, Phys. Rev. Lett. **82**, 855 (1999).
[36] Solution of catalyst-free BZ medium: $NaBrO_3 = 0.36M$, $CH_2(COOH)_2 = 0.0825M$, $H_2SO_4 = 0.18M$, BrMA= $0.165M$, and catalyst concentration of $0.004M$.
[37] R. M. Noyes, R. Field, and E. Koros, J. Am. Chem. Soc. **94**, 1394 (1972).
[38] A. N. Zaikin and A. M. Zhabotinsky, Nature (London) **225**, 535 (1970).
[39] W. H. Press, B. P. Flannery, S. A. Teukolsky, and W. T. Vetterling, *Numerical Recipes in C: The Art of Scientific Computing*, 2nd ed. (Cambridge University Press, England, 1992).
[40] Purchased from Aldrich (U.K.).
[41] T. Kusumi, T. Yamaguchi, R. R. Aliev, T. Amemiya, T. Ohmori, H. Hashimoto, and K. Yoshikawa, Chem. Phys. Lett. **271**, 355 (1997).
[42] See Supplemental Material at http://link.aps.org/supplemental/10.1103/PhysRevE.84.056110 for movies.